Effects of infiltration and evaporation on geosynthetic capillary barrier performance

John S. McCartney and Jorge G. Zornberg

Abstract: This study includes an experimental investigation of the transient movement of water in unsaturated soil layers underlain by a geocomposite drainage layer (GDL) during cycles of infiltration and evaporation. The distribution in volumetric water content with depth in a soil column having a height of 1350 mm underlain by a GDL was measured during transient infiltration. The capillary break effect was observed to affect the soil up to a height of 500 mm above the GDL, with an increase in volumetric water content up to 20% above that expected for the case of infiltration under a unit hydraulic gradient. Due to the long duration of this test (2000 h), a shorter 150 mm high soil column was also evaluated to investigate the soil–GDL hydraulic interaction during cycles of infiltration and evaporation. The capillary break was observed to have re-established itself after infiltration was stopped and the soil near the interface dried. The suction and volumetric water content measured in the soil at breakthrough were consistent after multiple cycles of wetting and drying. The conditions in the soil after each breakthrough event corresponded to the point on the drying-path water retention curve of the nonwoven geotextile where it transitioned from residual to saturated conditions.

Key words: geosynthetic capillary barriers, infiltration, unsaturated soils, geotextiles, geocomposites.

Résumé : Cet article présente une investigation expérimentale du mouvement transitoire de l'eau durant des cycles d'infiltration et d'évaporation dans des couches de sol non saturées placées sur une couche drainante en géocomposite (CDG). Une colonne de 1350 mm de haut avec une CDG à sa base a été installée afin de mesurer la distribution de la teneur en eau volumique selon la profondeur durant l'infiltration en régime transitoire. L'effet de bris capillaire affecte le sol jusqu'à 500 mm au-dessus de la CDG; ceci a été observé par une augmentation de la teneur en eau volumique jusqu'à 20% de plus que les valeurs attendues pour une infiltration sous un gradient hydraulique unitaire. Comme cet essai est de longue durée (2000 heures), une colonne plus courte, de 150 mm, a aussi été utilisée pour évaluer l'interaction hydraulique entre le sol et la CDG durant les cycles d'infiltration et d'évaporation. Le bris capillaire s'est rétabli suite à l'arrêt de l'infiltration et le sol près de la surface s'est asséché. Les succions et teneurs en eau mesurées dans le sol lors de la perte du bris capillaire étaient consistantes après plusieurs cycles de mouillage et séchage. Les conditions dans le sol après chacune des pertes du bris capillaire correspondent au point de la courbe de rétention d'eau en drainage du géotextile où il y a transition entre les conditions résiduelles et saturées.

Mots-clés : barrières capillaires en géosynthétique, infiltration, sols non saturés, géotextiles, géocomposites.

[Traduit par la Rédaction]

Introduction

Geocomposite drainage layers (GDLs) consisting of a geonet sandwiched between two nonwoven geotextiles are often used for leachate collection or leak detection in landfills, slope underdrains, subbase drainage in roadways, and drainage layers in mechanically stabilized earth walls. When water-saturated, the hydraulic conductivity of the nonwoven geotextile component of the geocomposite drainage layer (GDL) is higher than that of most fine-grained soils, in the absence of high normal compressive stresses or par-

J.S. McCartney.[1] Department of Civil, Environmental, and Architectural Engineering, University of Colorado at Boulder, UCB 428, Boulder, CO 80302, USA.
J.G. Zornberg. Civil Engineering Department – GEO, The University of Texas at Austin, 1 University Station C1792, Austin, TX 78712-0280, USA.

[1]Corresponding author (e-mail: john.mccartney@colorado.edu).

ticle clogging (Palmeira and Gardoni 2002). The high hydraulic conductivity of saturated nonwoven geotextiles leads to small head losses during drainage of water from soils. In contrast, when unsaturated, the hydraulic conductivity of geotextiles is often lower than that of most fine-grained soils (Morris 2000; Stormont and Morris 2000). Also, unsaturated nonwoven geotextiles only retain water by capillarity for values of suction, ψ, less than 1 kPa (Stormont et al. 1997; Knight and Kotha 2001; Nahlawi et al. 2007). A particular impact of the low hydraulic conductivity of geotextiles when unsaturated is that they may cause a capillary break effect when in contact with unsaturated soils (Clough and French 1982; Henry 1995).

The capillary break effect that develops at the interface of soils with different pore structures has been extensively investigated. A capillary break leads to a restriction in water flow from an unsaturated porous medium with relatively small pores into another unsaturated porous medium with relatively large pores. This phenomenon was first observed by Kisch (1959) and subsequently applied in many geotechnical applications (Rasmuson and Eriksson 1987; Nicholson et al. 1989; Barbour 1990; Shackelford et al. 1994; Woysh-

ner and Yanful 1995). The capillary break effect that develops in systems involving geosynthetics (e.g., GDLs) has only been evaluated more recently. Also in this case, the main effect of the capillary break effect on an unsaturated soil–GDL system is that a measurable amount of water will not flow from the soil into the underlying GDL until the suction, ψ, at their interface is reduced to a critical value referred to as the water-entry or breakthrough suction, ψ_b (Stormont 1995; Bouazza et al. 2006).

The capillary break effect has been observed to increase the water storage capacity of soils beyond the level that would normally drain under gravity (Stormont and Morris 1998; Khire et al. 2000). McCartney et al. (2005) observed that the volumetric water content at breakthrough, θ_b, for a silt–GDL system under steady infiltration was close to the silt's porosity. Furthermore, ψ_b for the silt–GDL system was found to be greater than that for a capillary barrier consisting of a silt–sand system, likely because of the greater porosity of the GDL's nonwoven geotextile compared with that of the sand.

The capillary break effect may have implications on the performance of slopes or walls if a GDL is expected to drain water from unsaturated fill in a similar way as saturated fill (Richardson 1997; Iryo and Rowe 2005). If a GDL is used as a liquid collection layer in landfill applications, it will only collect water when the overlying soil is nearly saturated, which has implications on the behavior of lysimeters and leak detection layers (Rowe and Iryo 2005; Zornberg and McCartney 2006). Conversely, the development of geosynthetic capillary barriers on moisture movement in soils may be useful to reach other engineering goals such as preventing frost heave (Henry and Holtz 2001), decreasing basal percolation in alternative landfill covers (Park and Fleming 2006; Zornberg and McCartney 2006), working as oxygen diffusion barriers (Yanful 1993; Bussiere et al. 2003), and minimizing moisture movement into roadway subgrades (Christopher et al. 2000).

Despite the wealth of research, there are still several issues that need to be resolved with respect to geosynthetic capillary barriers. Only limited laboratory studies on capillary barriers involving fine-grained soils have been performed due to the significant time requirements, especially for low infiltration rates (Stormont and Anderson 1999; Tami et al. 2004; Bathurst et al. 2007). There are several issues that have led to difficulties in the evaluation of field observations of soil layers underlain by geosynthetic capillary barriers. First, geosynthetic capillary barriers have been shown to behave differently from soil-only capillary barriers due to the high porosity of geotextiles (McCartney et al. 2005) as well as the presence of the geonet layer, whose large void space may influence the capillary break effect (McCartney et al. 2008). Second, methods developed to estimate the zone of influence of capillary barriers (Stormont and Morris 1998; Khire et al. 2000) have not been verified using experimental data for clays of low plasticity due to the significant requirements with respect to the soil column length and testing time. Third, although the capillary barrier is expected to re-establish after ψ at the interface decreases below ψ_b, the effects of wetting and drying cycles on the re-development of the barrier are uncertain. To address these needs, this study uses physical modeling to investigate the zone of influence of the geosynthetic capillary barrier on the volumetric water profile in the soil during infiltration as well as the conditions required for a geosynthetic capillary break effect to re-establish after capillary breakthrough.

Hydraulic characterization of materials

A Fabrinet geocomposite obtained from Gundle/SLT Environmental, Inc. (GSE) of Houston, Tex., was used in the laboratory tests conducted as part of this study. This GDL is composed of a 200-mil (5 mm) geonet sandwiched between two nonwoven geotextiles having a thickness of 2.54 mm each (GSE 2004). The nonwoven geotextiles have a mass per unit area 0.2 kg/m^2 and a fiber density of 910 kg/m^3. The porosity of the nonwoven geotextile under no confinement was calculated to be 0.91 using the porosity relationship defined for nonwoven geotextiles in Koerner (2005). This porosity is higher than that of most soils used in engineering applications (0.3 to 0.5).

The soil used in this study is classified as a low plasticity clay (CL) according to the "Unified Soil Classification System" (ASTM 2006) convention. The clay has a specific gravity of 2.7, a plasticity index of 12, and a liquid limit of 27. The clay was prepared in the laboratory using a pneumatic piston compactor, which is intended to replicate the compaction energy associated with hand-held vibratory plate compactors in the field. All soil specimens evaluated in this study were compacted at an optimal gravimetric water content of 11.5% (according to standard Proctor compaction tests (ASTM 2007)).

Water storage in an unsaturated porous medium is quantified by the water retention curve (WRC), which is the relationship between ψ and θ (or degree of saturation S_r) during drying or wetting. The water retention curves (WRCs) for the clay and geotextile of the GDL used in this study are shown in Fig. 1a. A hanging column apparatus (Haines 1930) was developed to define the drying-path and wetting-path WRCs for the nonwoven geotextile. The hanging column apparatus used in this study consisted of a Büchner funnel attached to an outflow burette constructed as a constant-head Mariotte bottle, which acted as the high-air entry porous disc (ψ_{aev} = 20 kPa). Further details of this setup are presented by McCartney et al. (2008). This setup allows measurement of the outflow volume with time from the geotextile during an applied ψ increment. The drying-path WRC data shown in Fig. 1a indicate that the nonwoven geotextile remains at a value of θ equal to the porosity until reaching an air-entry suction, ψ_{aev}, of 0.2 kPa. The geotextile reached residual saturation after applying a ψ value of 2.0 kPa. Subsequent re-wetting of the geotextile indicates that water re-enters the geotextile at a ψ value of approximately 0.5 kPa.

A pressure plate device developed based on the design of Wang and Benson (2004) was used to define the drying-path WRC for a clay specimen compacted to a porosity of 0.44. Unlike the geotextile, the soil was observed to show a more gradual decrease in θ with increasing ψ. At a ψ of 2.0 kPa, the geotextile was at residual saturation while the clay was still at a degree of saturation of approximately 0.95. The pressure plate was not used to determine the wetting curve for the soil, because the particular ψ from which re-wetting

occurs in field applications depends on atmospheric boundary conditions.

The hydraulic conductivity function (k-function) accounts for the change in the ratio between flow rate and total hydraulic gradient with increasing ψ (or decreasing θ). The k-functions shown in Fig. 1b for the different materials were predicted from the WRCs shown in Fig. 1a using the van Genuchten–Mualem (van Genuchten 1980) model. Measurements of the k-function for unsaturated geotextiles made by Morris (2000) and McCartney et al. (2008) indicate that the van Genuchten–Mualem model yields an acceptable prediction of the k-function shape for geotextiles. The hydraulic conductivity values of saturated soil and nonwoven geotextile specimens were measured using a flexible-wall permeameter. The specimens were back-pressure saturated with tap water as the permeating fluid. An effective stress of 7 kPa was used along with an average hydraulic gradient of 2.0, which are conditions representative of the base of a landfill cover system. The hydraulic conductivity of the geotextile is higher than that of the clay when saturated, but the opposite is true for ψ values greater than 2 kPa. At residual saturation, the hydraulic conductivity of a nonwoven geotextile predicted from the shape of the WRC using the van Genuchten–Mualem model (van Genuchten 1980) is less than 10^{-11} m/s. However, it is unlikely that there are continuous water pathways at residual saturation, so it may suffice to say that the geotextile is practically nonconductive for ψ values greater than 2 kPa.

The WRCs and k-functions in Figs. 1a and 1b can be used to predict ψ_b and the rate of fluid transport through the soil–GDL system. Analyses of hydraulic interaction between the two materials are founded on the principle of continuity of ψ at the interface, where ψ_b can be estimated using the WRC of the nonwoven geotextile. Specifically, ψ_b corresponds to the rapid change in slope from residual to saturated conditions of the coarse component of the system (Shackelford et al. 1994). This is ∼1.0 kPa for the nonwoven geotextile. Alternatively, the water-entry suction measured from the wetting curve of the geotextile WRC (0.5 kPa) may also be used as an estimate for ψ_b. It should also be noted that for ψ values below 1.0 kPa, the k-functions indicate that the hydraulic conductivity of the unsaturated nonwoven geotextile is greater than that of the unsaturated clay.

The value of ψ_b predicted using the approach suggested by Shackelford et al. (1994) was used to predict the volumetric water content of the soil at capillary breakthrough θ_b, for the situation of a constant infiltration rate. Most analyses of capillary barriers assume an initially unsaturated condition. For example, if the soil and geotextile are initially unsaturated with the same ψ of 100 kPa, the value of θ in the soil will be approximately 15% (a degree of saturation of 0.35), while the value of θ in the geotextile will be 0.0 (air dry). During infiltration from the surface of the soil layer, ψ in the soil will decrease. For the conditions of infiltration at an imposed (constant) flow rate under a unit hydraulic gradient, ψ in the soil will reach a value in equilibrium with the k-function. For example, steady infiltration at an imposed flow rate of 3.5×10^{-9} m/s under a unit gradient corresponds to a ψ of 24 kPa in the soil, according to its k-function in Fig. 1b. However, this only applies to locations in the

Fig. 1. Hydraulic characteristics for CL clay and nonwoven geotextile: (a) water retention curves; (b) predicted k-functions. Vol., volumetric.
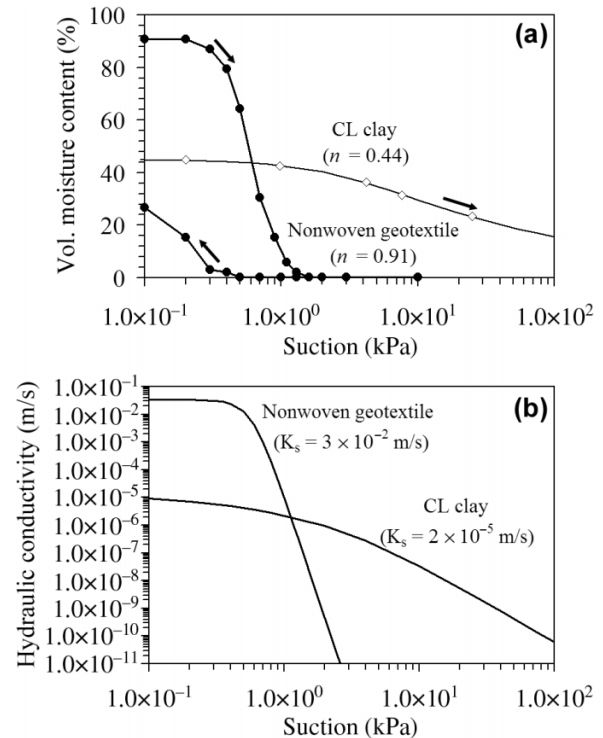

Fig. 2. Schematic profiles representing the zone of influence of the geosynthetic capillary barrier during steady-state infiltration: (a) matric suction; (b) volumetric water content.
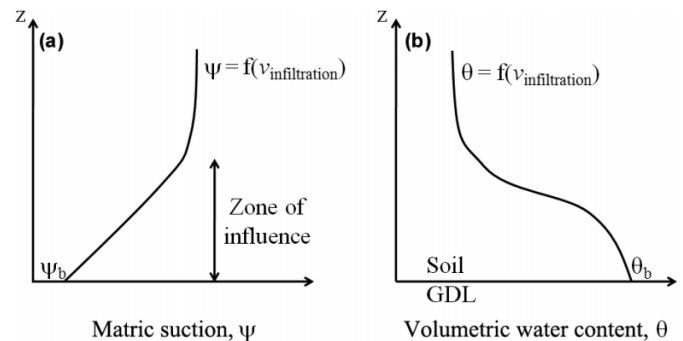

soil far from the geosynthetic capillary barrier. For breakthrough to occur, the value of ψ at the soil–GDL interface must decrease to a value of suction ψ_b of ∼1 kPa (note ψ_b shown in the geotextile WRC in Fig. 1a). The WRC of the CL clay indicates that this value of suction corresponds to a value θ_b of 43% (a degree of saturation of 0.95).

As a follow-up to the discussion in the previous paragraph, a schematic of the ψ profile at capillary breakthrough during steady-state infiltration is shown in Fig. 2a. The zone of influence of the capillary break depends on the breakthrough suction and the WRC of the soil overlying the GDL. A schematic of the θ distribution in a soil column at capillary breakthrough during steady-state infiltration is shown in Fig. 2b. Although the schematic illustration of θ shown in Fig. 2b is based on the assumption of a rate of in-

Fig. 3. Column A: (*a*) schematic cross section; (*b*) photo. All dimensions in millimetres. TDR, time domain reflectometry.
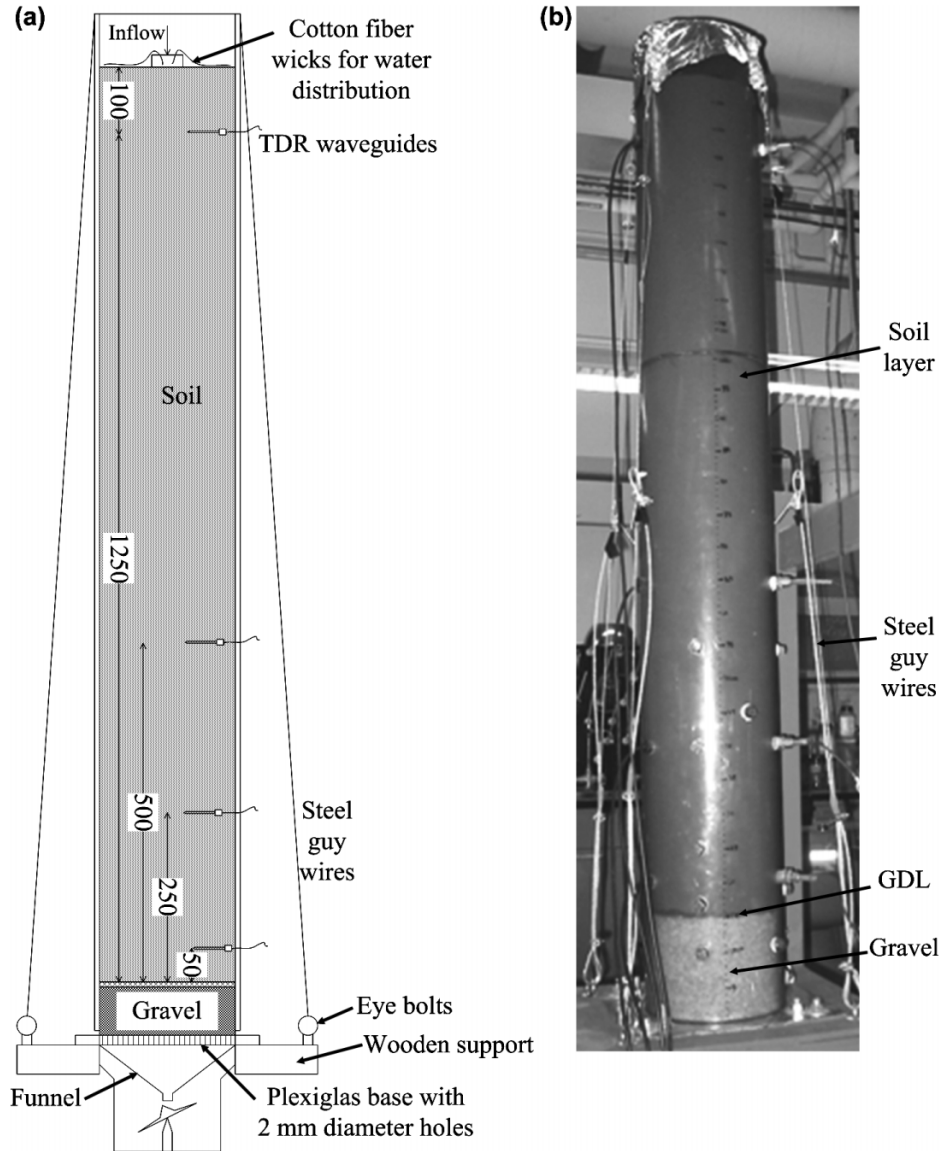
Fig. 4. Column B: (*a*) schematic cross section; (*b*) photo. All dimensions in millimetres.
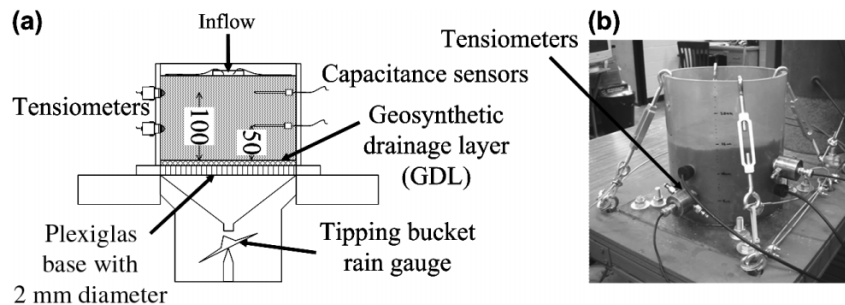
filtration less than the saturated hydraulic conductivity of the soil, the water storage in the CL clay layer above the capillary barrier is actually sensitive to the rate of infiltration (Choo and Yanful 2000). A special case would be the situation in which the infiltration rate is high enough to cause surface ponding. Bathurst et al. (2007, 2009) performed infiltration tests on soil–GDL profiles in which infiltration was

imposed by ponding water on the soil surface, and found that capillary breakthrough occurred when the wetting front (with a ψ value of approximately 0.0 kPa) reached the geosynthetic interface. This finding implies that an increase in θ will not be observed in any soil due to the capillary break effect for infiltration under ponding conditions. Siemens and Bathurst (2010) validated their experimental observa-

tions with numerical modeling of water flow using the hydraulic properties of the soil and GDL.

Laboratory testing program

Soil columns

Two soil columns were prepared in 203 mm diameter cylindrical polyvinyl chloride (PVC) tubes having a wall thickness of 12 mm. Tensioned steel wires were used to stabilize the column atop a Plexiglas outflow disc, which was supported by a wooden shelf. Column A was a 1350 mm thick clay layer compacted atop a GDL, which was underlain by a 100 mm thick layer of gravel. A schematic and picture of this column are shown in Fig. 3. The thickness of the clay layer in this column was selected to capture the expected zone of influence of the capillary barrier on the θ profile. Column B was a 125 mm thick clay layer compacted atop a GDL. A schematic and picture of this column are shown in Fig. 4. The thickness of the soil layer was selected to expedite the investigation of the influence of wet–dry cycles on capillary break formation.

The soil was placed into the columns in 25 mm lifts using a piston compactor. A thin film of vacuum grease was applied to the walls of the column before compaction to minimize side-wall leakage during infiltration and to reduce friction in case of volumetric changes in the soil. The porosity of the clay was 0.44 in column B and 0.49 in column A (corresponding approximately to a dry density equal to 70% of the maximum standard Proctor dry density). Despite a small difference in porosity, the results obtained from column A were expected to yield useful results to evaluate the impact of the geosynthetic capillary barrier on the water storage in the overlying soil column.

Inflow control and outflow measurement

The goal of the column flow tests conducted as part of this study was to permit free drainage of water through the unsaturated soil–GDL system. Consequently, the column was designed so that: (i) known water flow rates could be applied to the top of the soil; (ii) the bottom boundary would not provide impedance to water flow that exits from the base of the GDL; and (iii) air would be free to move from the soil surface or from the bottom of the GDL. These characteristics were different in other column tests reported in the literature, in which the water pressure was controlled at the upper and lower boundaries (i.e., constant head tests; Bathurst et al. 2007, 2009). To ensure that the bottom boundary of the column was free-draining, a honeycomb pattern of 1 mm diameter holes were drilled across the area of the plexiglas disc (Fig. 5a). An "O"-ring in a groove within the bottom edge of the PVC tube was used to prevent water from escaping from the interface between the PVC tube and the Plexiglas disc. The Plexiglas disc was supported atop a wooden shelf. Outflow from the holes in the Plexiglas disc was channeled into an aluminum funnel mounted directly below the Plexiglas disc, within a hole in the wooden shelf.

During infiltration, water was supplied to the soil surface using a peristaltic pump (Fig. 5b). Water from the peristaltic pump was supplied to an overflow cup, and was distributed to the soil surface using a network of cotton fiber wicks (Fig. 5d). This approach was found to provide uniform infil-

Fig. 5. Flow control system; (a) base support for columns; (b) peristaltic pump and inflow supply; (c) outflow monitoring setup; (d) inflow distribution system.
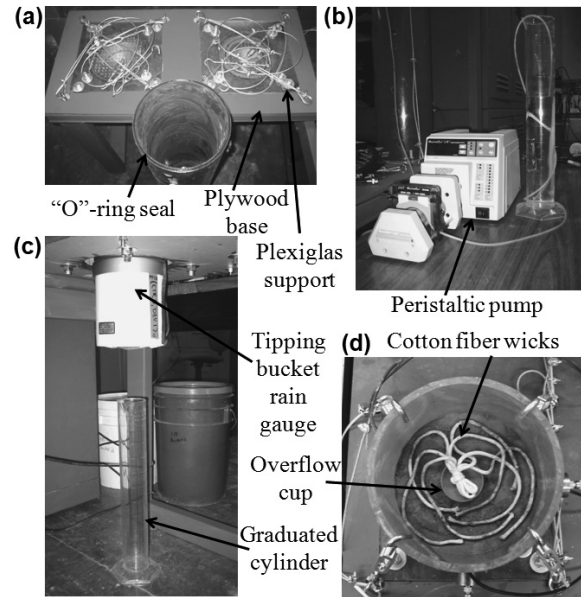
tration of water into the soil at a discharge velocity less than the hydraulic conductivity of the saturated clay. The outflow volume with time was measured using a tipping bucket rain gauge mounted below the funnel (Fig. 5c). This setup offers more control of the water flow processes in unsaturated soil layers than applying water to the soil by surface ponding (e.g., Bathurst et al. 2007).

During evaporation, an infrared lamp and fan were used to induce drying from the soil surface (Fig. 6b). This approach was not intended to replicate the actual energy supplied to the soil surface in the field to cause evaporation. Instead, this approach was used to provide a simple yet controlled means of inducing drying of the soil. A sheet of fiberglass insulation with a hole having the same diameter as the column was placed on top of the column to minimize heating of the column sides.

Instrumentation

The profiles of θ in the soil columns were monitored during infiltration and evaporation using time domain reflectometry (TDR) and capacitance probes. A MiniTRASE TDR system developed by SoilMoisture, Inc., Santa Barbara, Calif., was used in the monitoring system of column A (Fig. 7a), while ECH$_2$0-TE capacitance probes developed by Decagon Devices, Inc., Pullman, Wash., were used in the monitoring system of column B (Fig. 7b). Thermocouples embedded in the ECH$_2$0-TE probes were also used to measure the temperature profile within the soil column during evaporation. In both columns the water content sensors were placed in the middle of the soil lifts during compaction, and a rubber stopper was used to provide a seal between the sensor wire and ports in the column. The calibration relationships for these sensors are given by McCartney (2007).

Matric suction was measured in column B using flushing tensiometers that were specifically developed for this study.

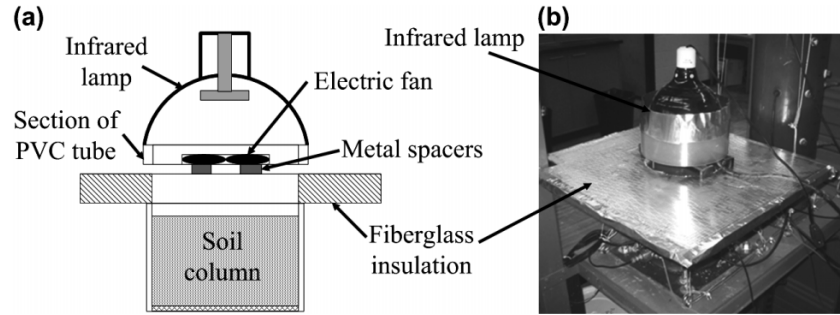**Fig. 6.** Evaporation setup: (*a*) schematic view; (*b*) photograph.

Fig. 7. Volumetric water content monitoring tools: (*a*) placement of TDR waveguide into soil lift in column A; (*b*) placement of capacitance probe into soil lift in column B.
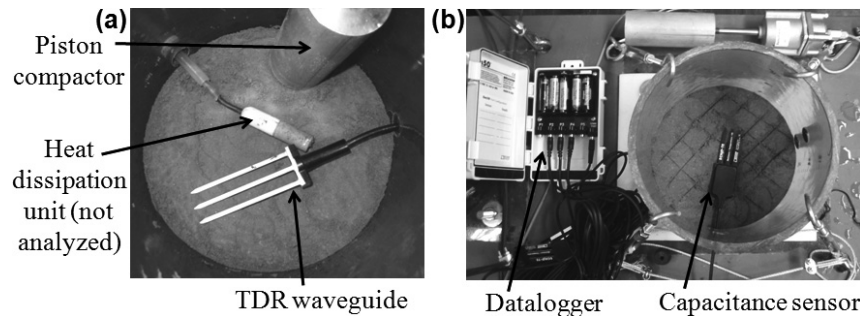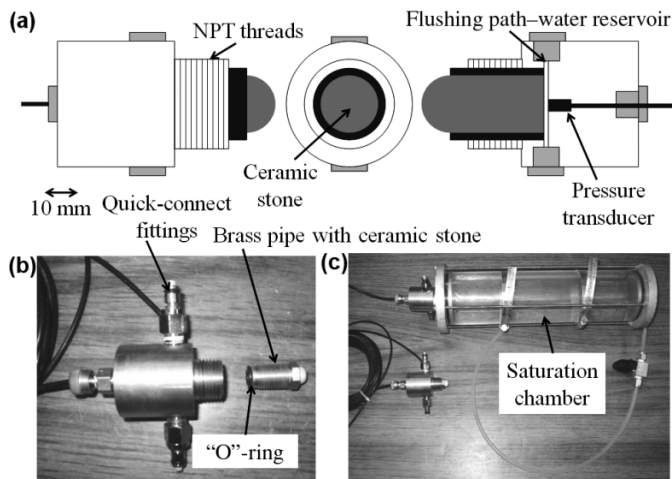

Fig. 8. Flushing tensiometer: (*a*) schematic views; (*b*) disassembled tensiometer showing sealing system for ceramic stone; (*c*) tensiometer attached to saturation chamber.

A schematic of the tensiometer is shown in Fig. 8*a*. A miniature pore pressure transducer (Druck PDCR-81) was used to monitor changes in pressure inside a water reservoir that was in direct contact with the soil via a ceramic stone having a high ψ_{aev} (Ridley and Burland 1996). As the soil dried, water was drawn out of the reservoir through the ceramic stone by capillarity, resulting in negative water pressure within the reservoir. The flushing ports aided in both facilitating initial saturation of the ceramic stone and in the removal of air bubbles in case of cavitation. The tensiometers were initially saturated by applying cycles of pressure (300 kPa) and high vacuum (–85 kPa) to a pressure reservoir shown in Fig. 8*b*. The tensiometers were considered saturated when the hydraulic conductivity of the porous ceramic stabilized after conducting successive pressure–vacuum cycles. The maximum ψ value measured using the tensiometer in this study was approximately 150 kPa, and cavitation was not noted during the infiltration and evaporation stages of this test. The tensiometers were screwed into the side wall of the PVC tube after compaction (as shown in Fig. 8*c*), which permitted intimate contact with the soil. More details of the tensiometers are given in McCartney (2007).

Experimental procedures

The geometry, soil conditions, stage duration, and boundary conditions for both soil columns are summarized in Table 1. The stage names include the cycle number and the stage type ("i" for infiltration or "e" for evaporation). The infiltration stages involved imposing a steady flow rate of an order of magnitude smaller than the saturated hydraulic conductivity of the clay, measuring the changes in θ and ψ with time as the wetting front progressed through the soil. An infiltration stage was completed when the outflow was the same as the inflow. The soil surface was covered during infiltration to maintain a constant relative humidity (~96%) in the air overlying the soil. The evaporation stages involved measurement of the surface temperature and relative humidity as well as profiles of temperature, T, θ, and ψ.

Column test results

Column A

The inflow and outflow data for column A during the infiltration and evaporation stages are shown in Fig. 9*a*. The slope of the relationship between the volume of inflow with time, divided by the area of the soil column, corresponds to the infiltration rate. The progress of the wetting front during

Table 1. Column descriptions and details of infiltration and evaporation stage.

Column name	Soil layer thickness (mm)	Compaction gravimetric water content (%)	Soil porosity, n	Saturated soil hydraulic conductivity (m/s)	Stage name	Stage description	Stage duration (h)	Infiltration rate (m/s)	Surface relative humidity (%)
A	1350	11.5	0.49	6.2×10^{-5}	1(i)	Infiltration	3106	3.4×10^{-9}	96
					1(e)	Evaporation	2179	0	13
					2(i)	Infiltration	819	3.4×10^{-8}	96
					2(e)	Evaporation	857	0	13
B	125	11.5	0.44	2.0×10^{-5}	1(i)	Infiltration	135	8.5×10^{-8}	96
					1(e)	Evaporation	101	0	13
					2(i)	Infiltration	93	8.5×10^{-8}	96
					2(e)	Evaporation	174	0	13
					3(i)	Infiltration	596	8.5×10^{-8}	96

the two infiltration stages, shown in Fig. 9b, indicates that the wetting front during stage 1(i) reached the base of the profile after approximately 1400 h from the start of infiltration. However, outflow was not collected until 1874 h. Consequently, the water that infiltrated into the soil from 1400 to 1874 h (an interval of 474 h) was stored within the soil. Less time was required for the wetting front to pass through the soil layer during infiltration stage 2(i) because the soil layer did not return to its original value of θ after evaporation stage 1(e). In addition to the more rapid progress of the wetting front through the soil layer during stage 2(i), breakthrough was observed after an interval of only 107 h (at a time of 5691 h) after the wetting front reached the base (at a time of 5584 h). Stage 2(i) was shorter than stage 1(i) because the soil was wetter near the base of the profile before infiltration was re-started in this stage.

The time series of θ shown in Fig. 9c provides insight into the reasons for the time delay between the arrival of the wetting front to the base of the column and the initiation of outflow during stage 1(i). As the wetting front passed the depths of each to the TDR waveguides, an increase in θ from 13.8% to ~24% was noted. A θ of 24% corresponds to the value of θ expected during infiltration under a unit hydraulic gradient at a rate equal to 3.4×10^{-9} m/s. After the wetting front reached the base of the profile, an increase in θ from 24% to 46% was measured by TDR 4 near the base of the profile (an elevation $z = 50$ mm measured from the column base). TDR 3 ($z = 250$ mm) and TDR 2 ($z = 500$ mm) also showed increases in θ, while TDR 1 ($z = 1250$ mm) did not show an increase in θ beyond approximately 24%.

The θ profiles during stage 1(i), shown in Fig. 9d, indicate that the soil within 500 mm of the base of the profile experienced an increase in θ beyond that expected during steady downward infiltration through the soil layer alone (e.g., had the GDL not been present). Consistent with the value of θ corresponding to the ψ_b value estimated from the hydraulic properties for the soil (Fig. 1), outflow was not observed to occur until the base of the soil layer reached a θ of 46% (S_r of 0.93). The shapes of the profiles of θ measured in column A for stage 1(i) are similar to those reported by McCartney and Zornberg (2004) for an unsaturated soil layer underlain by a GDL used as a lysimeter.

During the first evaporation stage 1(e) ($t = 3100$ h), the value of θ near the surface of the profile ($z = 1250$ mm) decreased from 24% to 20% during the first 100 h of evapora-

tion, followed by a more gradual decrease to 16% over 3 months. Slight decreases in θ were also noted at the depths of the other TDR waveguides during this stage, although these trends were probably due to gravity drainage, not evaporation. A delay in the decrease in θ was measured by the TDR waveguide near the base of the profile ($z = 50$ mm), which is likely due to a time-dependent decrease in the hydraulic conductivity of the geotextile as the ψ at the interface increased. The value of θ near the soil–geosynthetic interface eventually leveled off at 42%, likely due to reformation of the capillary break, which prevented further drainage of water from the soil. Measurements of gravimetric water content conducted by extracting soil from sampling ports indicated that the drying front progressed only 700 mm into the soil layer (i.e., $z = 650$ mm) during the 3 month long stage 1(e). The second cycle of infiltration (stage 2(i)) still led to an increase in θ at the base of the profile, from 42% to 45% before capillary breakthrough occurred, providing further evidence that the capillary break was re-established during the evaporation state 1(e). As the profile did not dry to its previous value of θ, the wetting front was observed to move about five times faster during stage 2(i).
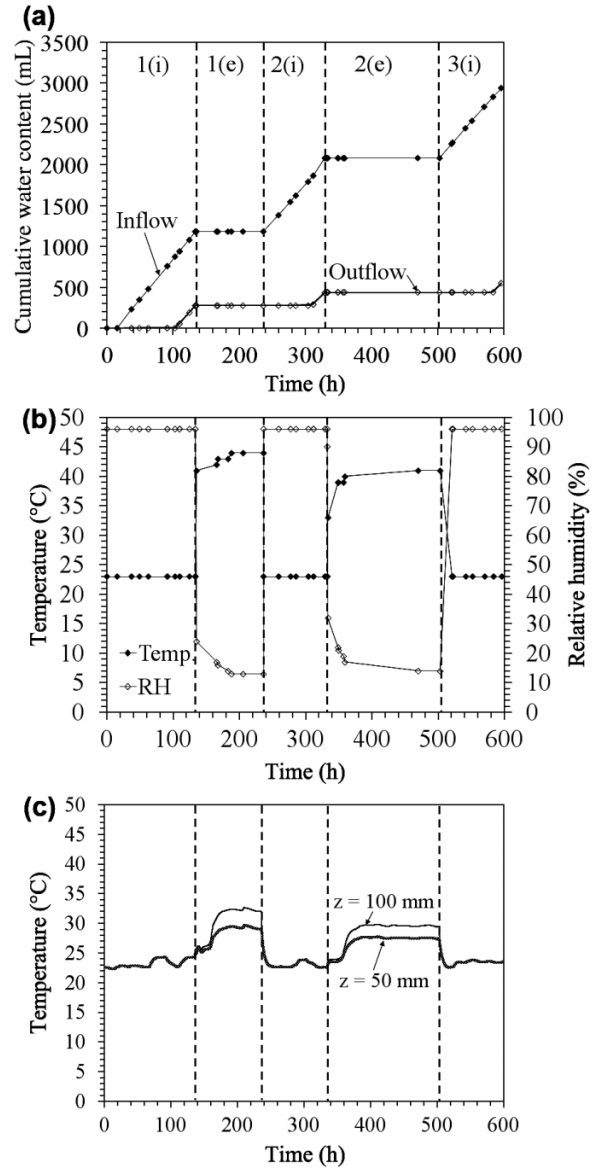
Column B

The inflow and outflow into column B are shown in Fig. 10a. Three infiltration stages were conducted, with intermediate evaporation stages. The infiltration stages were terminated when steady-state flow was observed, while the durations of the evaporation stages were varied to evaluate the impact of the amount of water removal on the behavior of the capillary barrier. The changes in temperature and relative humidity at the surface of the soil layer are shown in Fig. 10b, and changes in temperature at the elevations of the various capacitance sensors are shown in Fig. 10c. The infrared lamp led to an increase in surface temperature from 23 to 44 °C and a decrease in surface relative humidity from 96% to 13%. A relative humidity of 13% under a temperature of 44 °C corresponds to a steady-state suction boundary condition. The temperature in the soil increased significantly during early stages of evaporation, but reached steady-state conditions after 40 h of evaporation.

The bottom boundary (i.e., the GDL) had a significant effect on the profiles of θ and ψ in the soil due to the short length of the column. Based on the results from column A, a soil region of up to 500 mm of soil was expected to be affected by the capillary barrier. However, column B was only 125 mm thick. Regardless, this profile is particularly

Fig. 9. Results from profile A: (*a*) cumulative inflow and outflow (note: evaporation stages showed no infiltration); (*b*) progression of wetting front; (*c*) volumetric water content time series; (*d*) volumetric water content profiles.
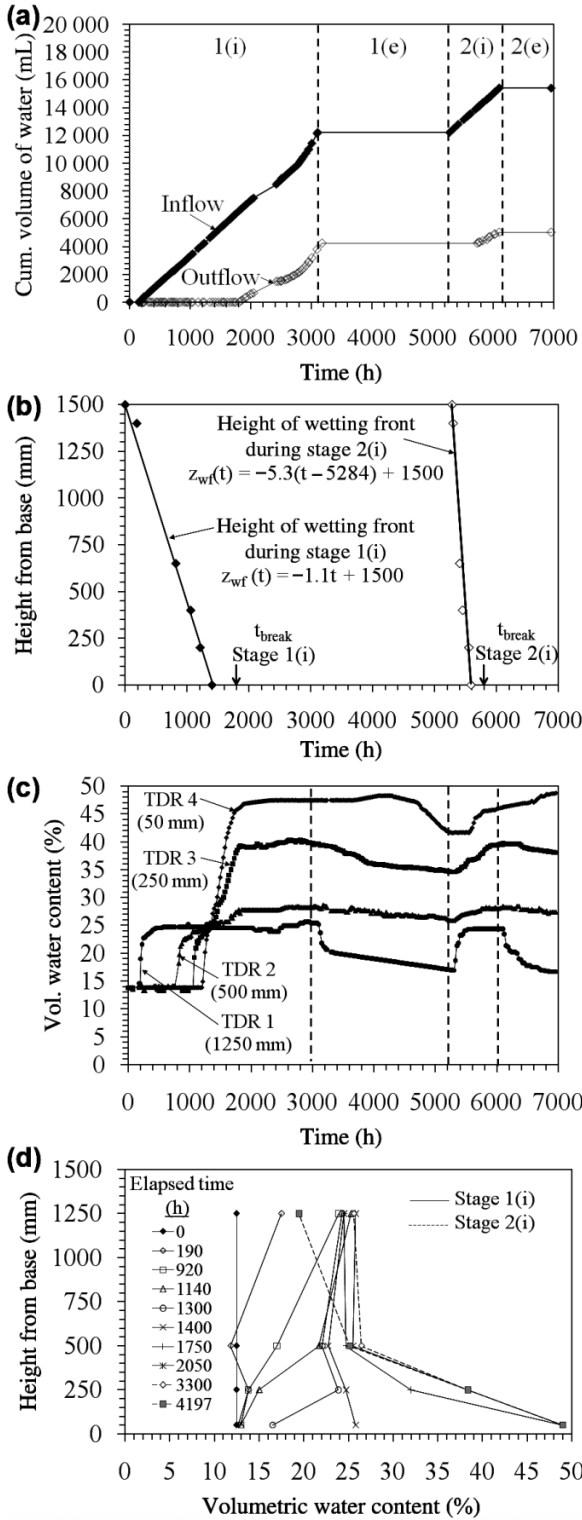

Fig. 10. Results from profile B: (*a*) cumulative inflow and outflow (note: evaporation stages showed no infiltration); (*b*) surface temperature and relative humidity (RH); (*c*) internal temperature.

of 50 mm was assumed to be representative of ψ at the interface. The tensiometers were still reaching equilibrium with an initial value of ψ in the soil after $\sim$25–45 h when the infiltration front passed their locations during stage 1(i). Nonetheless, the tensiometers showed a smooth decrease in ψ as the wetting front passed their locations. The times at which outflow was observed from the base of the column (i.e., capillary breakthrough) during each infiltration stage are shown by bold arrows in Fig. 11*a*. In stage 1(i), breakthrough occurred after 104 h when ψ in the soil at an elevation of 50 mm above the GDL reached 3.64 kPa. Consistent with the schematic ψ profile illustrated in Fig. 2*a*, the value of ψ_b was estimated as the measured ψ value at a height of 50 mm above the GDL, corrected by decreasing the elevation head of the tensiometers above the GDL. While an approximation, this correction considering a quasi-hydrostatic condition is deemed appropriate as the location of the GDL

useful to evaluate the conditions near the soil–geosynthetic interface during infiltration. The ψ time series for tensiometers located at elevations of 50 and 100 mm from the base are shown in Fig. 11*a*. The lower tensiometer at an elevation

Fig. 11. Results from profile B: (*a*) matric suction; (*b*) volumetric water content (bold arrows denote time of breakthrough inferred from initiation of outflow measurements).
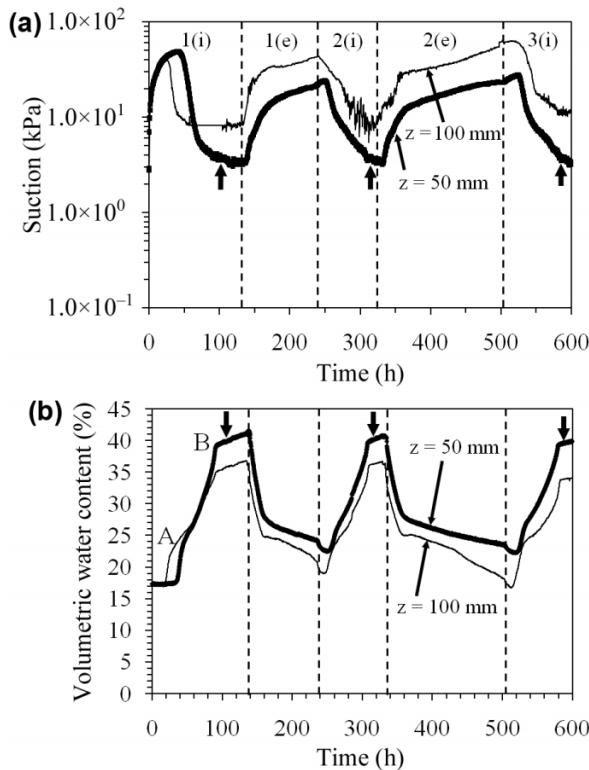
can be considered as a no-flow boundary until the moment of breakthrough. Accordingly, the value of ψ_b is 0.5 kPa lower than the measured value, or ∼3.0 kPa. After breakthrough, the tensiometers showed a continued decrease in ψ, likely due to the development of a ψ profile corresponding to steady-state flow with a nearly saturated bottom boundary.

The time series of θ for sensors at elevations of $z = 50$ and 100 mm from the base are shown in Fig. 11*b*. In general, the trends in θ measured using the capacitance sensors are consistent with the trends in ψ measured using the tensiometers. The value of θ at the wetting front is indicated by point A in Fig. 11*b*, which corresponds to the first plateau in θ after infiltration has started. The value of θ at the wetting front was approximately 24% for each infiltration stage. The upper portion of the column did not remain at the θ of the wetting front due to the shorter height of this column. Instead, the value of θ throughout the soil layer increased due to the accumulation of water above the GDL induced by the capillary break. Capillary breakthrough occurred when the sensor at $z = 50$ mm reached a θ of 40%, slightly after the second plateau in θ (point B in Fig. 11*b*). The value of θ at this point continued to increase up to 43% after outflow started, indicating development of a profile of θ that was in equilibrium for the imposed infiltration rate.

After reaching steady-state outflow, inflow was stopped and the evaporation system was used to start surface evaporation. During the first 20 h of stage 1(e), a significant decrease in θ (from 43% to 25%) was observed. A less pronounced decrease in θ (from 25% to 21%) was observed

over the next 80 h of drying. The imposed boundary condition resulted in a gradient in θ (and ψ) across the specimen. After the initial rapid decrease in θ, drying continued at a slower rate, probably because the thermal conductivity and hydraulic conductivity of the surface layer of soil decreased as the soil reached lower values of θ. Desiccation was not observed during evaporation, so water did not exit from deeper in the soil layer by mechanisms other than diffusive flow through the unsaturated surface crust.

The values of θ and ψ in the lower section of the profile did not return to their original values after the evaporation phase, but the value of ψ remained above the value expected for capillary breakthrough. Accordingly, after subsequent wetting of the profile in stage 2(i), the values of θ and ψ at capillary breakthrough were similar to the values observed during stage 1(i). This indicates that as long as the value of ψ at the soil–geosynthetic interface decreases below ψ_b during evaporation, the capillary break effect is expected to develop during subsequent infiltration. To evaluate the impact of additional drying of the soil layer, evaporation stage 2(e) was conducted during a period 75% longer than the previous cycle. Other than delaying the time for breakthrough to occur in the third infiltration stage, the amount of water removal had no impact on the performance of the capillary barrier, and the values of θ and ψ measured at breakthrough at infiltration stage 3(i) were similar to those observed in the earlier stages. The elevated temperature was found to impact the magnitude of θ and ψ measured using the tensiometer and capacitance sensors, respectively, by ∼5%. However, as the main objective of column B was to assess the values of θ and ψ at capillary breakthrough during infiltration, the impact of temperature on the values of θ and ψ during evaporation was deemed acceptable.

Discussion of results

The results obtained during the infiltration and evaporation stages of profiles A and B are summarized in Table 2. The speed of the wetting fronts tended to increase with each cycle because θ did not return to its initial value at the end of each evaporation stage. Similar observations can be made regarding the time required to reach steady-state infiltration. The speed of the evaporation front was calculated from the difference in times between responses of the capacitance sensors to the imposed evaporation. The calculated speeds were similar for the two evaporation stages.

The values of θ and ψ at the infiltration front (24% and 25 kPa, respectively) are similar for columns A and B as the inflow rates used are similar, and because the difference in hydraulic properties for the soils with different porosities are likely similar at higher ψ values (McCartney 2007). Also, breakthrough for each wet–dry cycle occurred at a similar degree of saturation in both profiles (0.91). The ψ value measured at breakthrough from column B (3.1 kPa) is on the same order of magnitude as the estimated value predicted from the drying WRC for the geotextile (1.0 kPa).

The transient WRCs during the first two wetting and drying cycles obtained from the capacitance sensor and tensiometer data are shown in Figs. 12*a* and 12*b*. Similar transient WRCs were observed for both cycles. The wetting and drying paths are scanning curves, which follow the shape of the drying-path WRC for the clay, indicating that

Table 2. Summary of results for columns A and B.

Column name	Stage	Speed of wetting front (m/s)	Suction at wetting front (kPa)	Volumetric water content at wetting front (%)	Time until steady-state infiltration (h)	Breakthrough suction (kPa)	Breakthrough moisture content (%)	Speed of evaporation front (m/s)	Depth of evaporation front (mm)
A	1	2.7×10^{-7}	Not measured	24.7	1874	N/A	46.2	0	700
	2	1.0×10^{-6}	Not measured	24.4	453	N/A	45.6	0	500
B	1	9.6×10^{-7}	21.1	24.3	105	2.65	40.2	3.5×10^{-6}	125
	2	1.5×10^{-6}	25.0	24.1	75	2.75	40.5	3.1×10^{-6}	125
	3	1.8×10^{-6}	25.8	24.2	83	2.65	39.6	0	125

the drying WRC for the soil provides a good estimate of the value of θ in the soil at capillary breakthrough. The differences between the drying WRC and the in situ WRCs may possibly be due to the differences in the water flow processes. The drying WRC was defined using axis translation and transient flow toward equilibrium conditions, while the in situ WRCs were defined by infiltration. The flow processes may have occurred through different pores in the soil layer. Only minor hysteresis is observed in the transient WRCs. The only exception is the data from the sensors at $z = 100$ mm in cycle 1, although the differences are likely due to variability in the tensiometer measurements near saturation. Less hysteresis is observed in cycle 2 than in cycle 1.
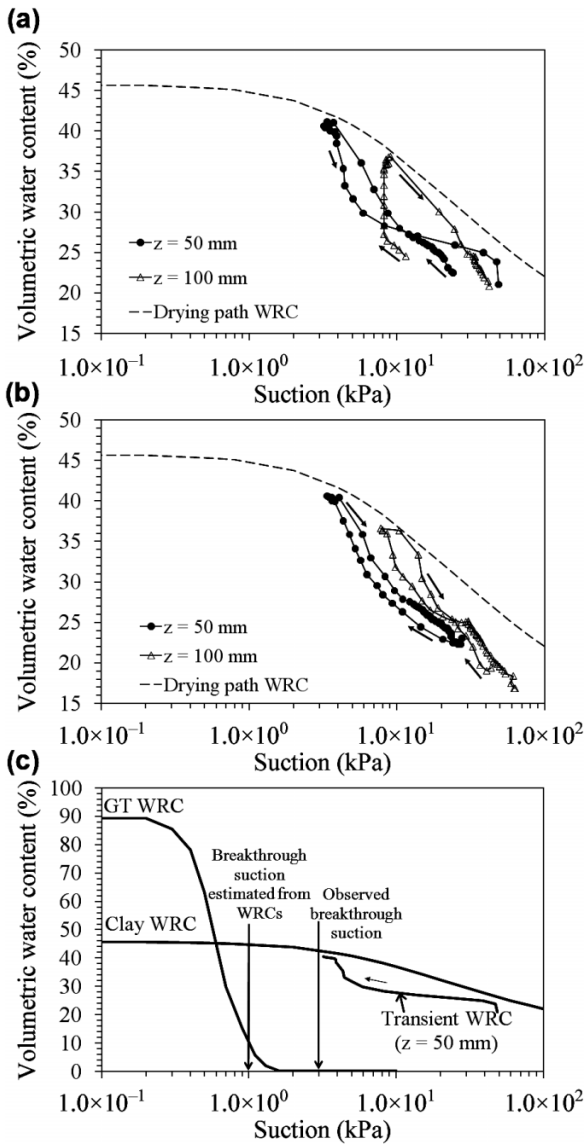
The left-most point on the WRCs in Figs. 12*a* and 12*b* defined using the sensors at $z = 50$ mm correspond approximately to the conditions during capillary breakthrough (i.e., without considering the difference in elevation head). The drying curves from both cycles with the estimated and actual ψ_b values (adjusted for elevation head) are shown in Fig. 12*c*. The differences between these values could be due to intrusion of soil particles into the geotextile during compaction, compression of the geotextile or impact of the underlying geonet on flow out of the geotextile after water has broken through from the soil. With respect to the last possibility, a capillary break would be expected to occur between the geotextile and the geonet. However this interface is considered a relatively "brittle" capillary barrier because of the small thickness of the geotextile and the high hydraulic conductivity of the geotextile once water has broken through from the soil. Nonetheless, the results in Fig. 12*c* indicate that the drying-path WRC for the geotextile can be used to estimate the ψ_b for unsaturated soil–geosynthetic systems. The suitability of the drying curves in predicting the hydraulic interaction between unsaturated soils and geosynthetics has practical implications, as these curves are generally the most common unsaturated properties measured in geotechnical practice. Also, these curves are straightforward to obtain without the need for instrumentation or expensive equipment.

Conclusions

This study includes an experimental evaluation of water flow processes in unsaturated soil layers underlain by geosynthetic capillary barriers. Specifically, controlled infiltration and evaporation tests were performed on two soil columns having different thicknesses to evaluate the zone of influence of the capillary break effect on the volumetric water content profile and the impact of wetting and drying on the suction and volumetric water content at capillary breakthrough. Specific conclusions drawn from this study include the following:

- For the case of steady infiltration into an initially unsaturated soil at an imposed infiltration rate below the saturated hydraulic conductivity, the capillary barrier was found to lead to θ values in a zone above the GDL (500 mm for the low-plasticity clay evaluated in this study) that are higher than the values corresponding to infiltration under a unit hydraulic gradient.
- Evaporation induced using heat lamps after the initial in-

Fig. 12. Comparison between drying-path and transient WRCs for the CL clay: (*a*) cycle 1; (*b*) cycle 2; (*c*) predicted and measured breakthrough suction values. Arrows indicate infiltration (decreasing suction) or evaporation (increasing suction).

- After repeated wet–dry cycles, capillary breakthrough was observed to occur at the same ψ and θ values in the test columns.
- For both the soil and geosynthetic, the drying-path water retention curve provides a good basis to assess the hydraulic interaction between the soil and geosynthetic, even for infiltration processes. The ψ value measured at breakthrough was found to correspond to the value of ψ at the transition from residual to saturated conditions in the drainage water retention curves for the nonwoven geotextile. Similarly, the water retention curve for the soil was observed to provide a good indication of the degree of saturation in the soil at capillary breakthrough. Specifically, the WRCs were used to estimate that capillary breakthrough would occur at a degree of saturation in the soil of 0.95, while the column test indicated that breakthrough occurred at a degree of saturation in the soil of 0.91.
- Theoretical approaches to define the zone of influence of the geosynthetic capillary barrier on the θ profile in an overlying soil layer match well with observations from the column tests.

Acknowledgement

References

ASTM. 2006. Standard practice for classification of soils for engineering purposes (Unified Soil Classification System). ASTM standard D2487. American Society for Testing and Materials, West Conshohocken, Penn.

ASTM. 2007. Standard test methods for laboratory compaction characteristics of soil using standard effort (12 400 ft-lbf/ft3 (600 kN·m/m³)). ASTM standard D698. American Society for Testing and Materials, West Conshohocken, Penn.

Barbour, S.L. 1990. Reduction of acid generation in mine tailings through the use of moisture-retaining cover layers as oxygen barriers: Discussion. Canadian Geotechnical Journal, **27**(3): 398–401. doi:10.1139/t90-051.

Bathurst, R., Ho, A.F., and Siemens, G. 2007. A column apparatus for investigation of 1-D unsaturated–saturated response of sand-geotextile systems. Geotechnical Testing Journal, **30**(6): 433–441. doi:10.1520/GTJ100954.

Bathurst, R.J., Siemens, G., and Ho, A.F. 2009. Experimental investigation of infiltration ponding in one-dimensional sand–geotextile columns. Geosynthetics International, **16**(3): 158–172. doi:10.1680/gein.2009.16.3.158.

Bouazza, A., Zornberg, J.G., McCartney, J.S., and Nahlawi, H. 2006. Significance of unsaturated behaviour of geotextiles in earthen structures. Australian Geomechanics, **41**(3): 133–142.

Bussière, B., Aubertin, M., and Chapuis, R.P. 2003. The behavior of inclined covers used as oxygen barriers. Canadian Geotechnical Journal, **40**(3): 512–535. doi:10.1139/t03-001.

Choo, L.P., and Yanful, E.K. 2000. Water flow through cover soils using modeling and experimental methods. Journal of Geotechnical and Geoenvironmental Engineering, **126**(4): 324–334. doi:10.1061/(ASCE)1090-0241(2000)126:4(324).

Christopher, B.R., Hayden, S.A., and Zhao, A. 2000. Roadway base and subgrade geocomposite drainage layers. *In* Testing and Performance of Geosynthetics in Subsurface Drainage. STP 1390. *Edited by* L.D. Suits, J.B. Goddard, and J.S. Baldwin. American

filtration stage was observed not to lead to a significant decrease in soil θ beyond a certain depth under the soil surface (600 mm in this study). Drainage of water from the base of the columns was observed to occur at a decreasing rate until the capillary break was re-established at a θ close to that observed at breakthrough (approximately 42% or $S_r = 0.85$ in this study).

- Re-establishment of the capillary break was observed to rely only on a decrease in ψ at the interface to values beyond ψ_b. However, the rate at which the wetting front moves through the soil during subsequent infiltration stages was found to increase. Furthermore, the amount of time required before capillary breakthrough occurred during this infiltration stage was found to decrease during the subsequent infiltration stages. This was because the amount of water in the soil did not decrease significantly during the evaporation stages.

Society for Testing and Materials (ASTM), West Conshohocken, Penn. pp. 35–51.

Clough, I.R., and French, W.J. 1982. Laboratory and field work relating to the use of geotextiles in arid regions. *In* Proceedings of the 2nd International Conference on Geotextiles, Las Vegas, Nev., 1–6 August 1982. Industrial Fabric Association International, Roseville, Minn. Vol. 2, pp. 447–452.

GSE. 2004. GSE Fabrinet geocomposite – product data sheet. GSE, Inc., Houston, Tex.

Haines, W.B. 1930. Studies in the physical properties of soil. V. The hysteresis effect in capillary properties, and the modes of moisture distribution associated therewith. The Journal of Agricultural Science, **20**(01): 97–116. doi:10.1017/S002185960008864X.

Henry, K.S. 1995. The use of geosynthetic capillary barriers to reduce moisture migration in soils. Geosynthetics International, **2**(5): 883–888.

Henry, K.S., and Holtz, R.D. 2001. Geocomposite capillary barriers to reduce frost heave in soils. Canadian Geotechnical Journal, **38**(4): 678–694. doi:10.1139/cgj-38-4-678.

Iryo, T., and Rowe, R.K. 2005. Infiltration into an embankment reinforced by nonwoven geotextiles. Canadian Geotechnical Journal, **42**(4): 1145–1159. doi:10.1139/t05-035.

Khire, M.V., Benson, C.H., and Bosscher, P.J. 2000. Capillary barriers: Design variables and water balance. Journal of Geotechnical and Geoenvironmental Engineering, **126**(8): 695–708. doi:10.1061/(ASCE)1090-0241(2000)126:8(695).

Kisch, M. 1959. The theory of seepage from clay-blanketed reservoirs. Géotechnique, **9**(1): 9–21. doi:10.1680/geot.1959.9.1.9.

Knight, M.A., and Kotha, S.M. 2001. Measurements of geotextile–water characteristic curves using a controlled outflow capillary pressure cell. Geosynthetics International, **8**(3): 271–282.

Koerner, R.M. 2005. Designing with geosynthetics. 5th ed. Prentice Hall, Upper Saddle River, N.J.

McCartney, J.S. 2007. Determination of the hydraulic characteristics of unsaturated soils. Ph.D. dissertation. The University of Texas at Austin, Austin, Tex.

McCartney, J.S., and Zornberg, J.G. 2004. Use of moisture profiles and lysimetry to assess evapotranspirative cover performance. *In* Proceedings of the 5th International Ph.D. Symposium in Civil Engineering, Delft, the Netherlands, 16–19 June 2004. *Edited by* J. Blaauwendraad, T. Scarpas, B. Snijder, and J. Walraven. Taylor & Francis, London. pp. 961–969.

McCartney, J.S., Kuhn, J.A., and Zornberg, J.G. 2005. Geosynthetic drainage layers in contact with unsaturated soils. *In* Proceedings of the 16th International Congress of Soil Mechanics and Geotechnical Engineering, Osaka, Japan, 12–16 September 2005. Millpress, Amsterdam, the Netherlands.

McCartney, J.S., Villar, L.F.S., and Zornberg, J.G. 2008. Nonwoven geotextiles as hydraulic barriers to capillary rise. *In* Proceedings of GeoAmericas 2008, the First PanAmerican Geosynthetics Conference and Exhibition, Cancún, Mexico, 2–5 March 2008. pp. 252–261.

Morris, C.E. 2000. Unsaturated flow in nonwoven geotextiles. *In* Proceedings of GeoEng 2000: an International Conference on Geotechnical and Geological Engineering, Melbourne, Australia, 19–24 November 2000. Technomic Publishing Company, Lancaster, Penn. Vol. 2, p. 322.

Nahlawi, H., Bouazza, A., and Kodikara, J.K. 2007. Characterisation of geotextiles water retention using a modified capillary pressure cell. Geotextiles and Geomembranes, **25**(3): 186–193. doi:10.1016/j.geotexmem.2006.12.001.

Nicholson, R.V., Gillham, R.W., Cherry, J.A., and Reardon, E.J. 1989. Reduction of acid generation in mine tailings through the use of moisture-retaining cover layers as oxygen barriers. Canadian Geotechnical Journal, **26**(1): 1–8. doi:10.1139/t89-001.

Palmeira, E., and Gardoni, M. 2002. Drainage and filtration properties of non-woven geotextiles under confinement using different experimental techniques. Geotextiles and Geomembranes, **20**(2): 97–115. doi:10.1016/S0266-1144(02)00004-3.

Park, K.D., and Fleming, I.R. 2006. Evaluation of a geosynthetic capillary barrier. Geotextiles and Geomembranes, **24**(1): 64–71. doi:10.1016/j.geotexmem.2005.06.001.

Rasmuson, A., and Eriksson, J.-C. 1987. Capillary barriers in covers for mine tailing dumps. National Swedish Environmental Protection Board Report 3307. Royal Institute of Technology, Stockholm, Sweden.

Richardson, G.N. 1997. Fundamental mistakes in slope design. Geotechnical Fabrics Report. **15**(2): 15–17.

Ridley, A.M., and Burland, J.B. 1996. A pore water pressure probe for the in situ measurement of a wide range of soil suctions. *In* Advances in Site Investigation Practice, Proceedings of an International Conference, London, 30–31 March 1995. *Edited by* C. Craig. Thomas Telford, London. pp. 510–520.

Rowe, K.R., and Iryo, T. 2005. Effects of geosynthetics on the hydraulic performance of leak detection systems. Canadian Geotechnical Journal, **42**(5): 1359–1376. doi:10.1139/t05-059.

Shackelford, C.D., Chang, C.-K., and Chiu, T.-F. 1994. The capillary barrier effect in unsaturated flow through soil barriers. *In* Proceedings of the 1st International Conference on Environmental Geotechnics, Edmonton, Alta., 11–14 July 1994. BiTech Publishers, Richmond, B.C. pp. 789–793.

Siemens, G., and Bathurst, R.J. 2010. Numerical parametric investigation of infiltration in one-dimensional sand–geotextile columns. Geotextiles and Geomembranes, **28**: 460–474. doi:10.1016/j.geotexmem.2009.12.009 .

Stormont, J.C. 1995. The performance of two capillary barriers during constant infiltration. *In* Landfill closures – Environmental protection and land recovery. GSP No. 53. *Edited by* R.J. Dunn and U.P. Singh. American Society of Civil Engineers (ASCE), New York. pp. 77–92.

Stormont, J., and Anderson, C. 1999. Capillary break effect from underlying coarser soil layer. Journal of Geotechnical and Geoenvironmental Engineering, **125**(8): 641–648. doi:10.1061/(ASCE)1090-0241(1999)125:8(641).

Stormont, J.C., and Morris, C.E. 1998. Method to estimate water storage capacity of capillary barriers. Journal of Geotechnical and Geoenvironmental Engineering, **124**(4): 297–302. doi:10.1061/(ASCE)1090-0241(1998)124:4(297).

Stormont, J.C., and Morris, C.E. 2000. Characterization of unsaturated nonwoven geotextiles. *In* Advances in Unsaturated Geotechnics. *Edited by* C. Shackelford, S. Houston, and N.-Y. Chang. American Society of Civil Engineers (ASCE), Reston, Va. pp. 153–164.

Stormont, J.C., Henry, K.S., and Evans, T.M. 1997. Water retention functions of four non-woven polypropylene geotextiles. Geosynthetics International, **4**(6): 661–672.

Tami, D., Rahardjo, H., Leong, E.-C., and Fredlund, D.G. 2004. A physical model for sloping capillary barriers. Geotechnical Testing Journal, **27**(2): 1–11. doi:10.1520/GTJ11431.

van Genuchten, M. 1980. A closed-form equation for predicting the hydraulic conductivity of unsaturated soils. Soil Science Society of America Journal, **44**: 892–898.

Wang, X., and Benson, C.H. 2004. Leak-free pressure plate extractor for measuring the soil water characteristic curve. Geotechnical Testing Journal, **27**(2): 163–172. doi:10.1520/GTJ11392.

Woyshner, M.R., and Yanful, E.K. 1995. Modelling and field measurements of water percolation through an experimental soil

cover on mine tailings. Canadian Geotechnical Journal, **32**(4): 601–609. doi:10.1139/t95-062.

Yanful, E.K. 1993. Oxygen diffusion through soil covers on sulphidic mine tailings. Journal of Geotechnical Engineering, **119**(8): 1207–1228. doi:10.1061/(ASCE)0733-9410(1993)119:8(1207).

Zornberg, J.G., and McCartney, J.S. 2006. Evapotranspirative cover systems for waste containment. *In* Handbook of groundwater engineering. *Edited by* J. Delleur. CRC Press, Boca Raton, Fla. Vol. 2, pp. 34-1–34-31.

List of symbols

K_s saturated hydraulic conductivity (m/s)
n porosity
T temperature (K)
t time
t_{break} breakthrough time (h)
S_r degree of saturation (dimensionless)
$v_{infiltration}$ infiltration rate (m/s)
z elevation
$z_{wf}(t)$ depth of the wetting front (m)
θ volumetric water content (%)
θ_b volumetric water content at breakthrough (%)
ψ matric suction (kPa)
ψ_{aev} air-entry suction for a porous material (kPa)
ψ_b matric suction at capillary breakthrough (kPa)